JOURNAL OF SYNCHROTRON RADIATION
ISSN 1600-5775

Numerical analysis of brilliance and coherent photon flux of segmented undulator radiation based on statistical optics

Hao-Wen Luo,[a,b]* Ting-Yi Chung,[b] Chih-Hao Lee[a] and Ching-Shiang Hwang[b,c]*

[a]Engineering and System Science, National Tsing Hua University, No. 101, Section 2, Guangfu Road, East District, Hsinchu City 30013, Taiwan, [b]National Synchrotron Radiation Research Center, 101 Hsin-Ann Road, Hsinchu Science Park, Hsinchu City 30076, Taiwan, and [c]Electrophysics, National Chiao Tung University, 1001 University Road, Hsinchu City 30010, Taiwan. *Correspondence e-mail: luo.hw@nsrrc.org.tw, cshwang@nsrrc.org.tw

Received 3 August 2018
Accepted 12 November 2018

Edited by I. Lindau, SLAC/Stanford University, USA

Keywords: Wigner distribution function; brilliance; transverse coherence; double mini-β_y lattice; segment undulator.

A method based on wave optics together with electron tracking is used to analyze synchrotron radiation from a segmented undulator in a double or multi mini-β function lattice storage ring. Radiation brilliance and transverse coherence features are investigated, where the former is calculated with the Wigner distribution function and the latter is evaluated by integrating the photon flux and cross-spectral density to exhibit the coherent flux and overall degree of coherence. To be specific, radiation properties for a single undulator in a typically single mini-β function and a tandem undulator in a double mini-β_y lattice are compared in this work. As a result, both, brilliance and coherent flux can be enhanced by a second tandem undulator at the Taiwan Photon Source.

1. Introduction

There has been significant progress in generating high-brilliant and transverse coherent synchrotron radiation (SR) in storage rings by reducing the electron beam emittance (Eriksson *et al.*, 2016; Willeke, 2015; Kuo *et al.*, 2015) and by installing very long undulators (Hara *et al.*, 2002; Yamamoto *et al.*, 2014). The first method has been encouraged because of progress in synchrotron technologies, such as lattice design, magnets, vacuum system and the injection schemes. Upgrade projects or new facilities are proposed or are under construction. The second approach mainly relies on insertion device (ID) technology. Even though a continuous-segment ID in a very long straight section is desired, it is convenient to separate a long ID into shorter segments for a number of practical reasons. First, there is the electron lifetime degradation due to elastic scattering with residual gas molecules and the function of β_y in the narrow gap of an undulator, which pushes for a shorter length of the undulator. Second, several essential components requiring space, such as vacuum pumps, beam diagnostic elements, steering and quadrupole magnets, must be installed for normal beam operation along the ID.

The technologies of segmented undulators have been applied at SPring-8 (Yamamoto *et al.*, 2014), ESRF (Chavanne *et al.*, 1996) and BESSY II (Reichardt *et al.*, 2001). At ESRF, the measured angular flux density from two 1.6 m-long segments compared with a single segment increases by a factor of 3.1 at 3.5 keV and 2.3 at 20 keV (Onuki & Elleaume, 2003). The angular flux density, being less than the ideal factor of four, is photon-energy-dependent and depends on the emittance and energy spread of the electron beam and on perfect

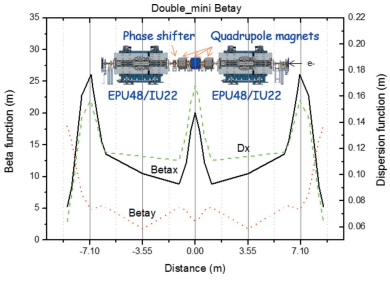

matching of the electron and photon phases in the transverse phase space. To observe the interference effect, it is necessary to install a monochromator to improve the spectral resolution. In general, the phase matching in the transverse phase space decreases with increasing photon energy. The phase matching of segmented undulator radiation is a sensitive factor but has never been described rigorously in terms of photon-energy-dependent degradation of SR. Here we pose one question: how to improve the SR brilliance for high photon energies? A straightforward method is to increase the overlapping region of the two transverse phase spaces by minimizing the β-function at the location of each segmented undulator (Chiu *et al.*, 2010) (see Fig. 1). Installation of quadrupoles, however, raises two flags. First, the electron beam deflection and displacement introduced by the quadrupoles should be kept small to preserve the spatial overlap of the photon beams emitted from both segments. Second, the path length of the electron beam should be adjusted so as to retain temporal matching between radiation fields emitted from both segments. The first case relates to the electron beam quality and beam dynamics control (Baron *et al.*, 2016), yet our work will focus on the SR performance for a perfect transverse alignment. Due to the fact that quadrupoles will affect phase matching, we leave most of the electron deflection issues to the qualitative discussion in Section 5.

The SR brilliance is a figure of merit for a light source, indicating how well SR can be focused (Geloni *et al.*, 2015). A typical evaluation of the SR brilliance emitted from an electron beam passing through an undulator is to apply a convolution of the Wigner distribution function (WDF) of the photon beam from a single electron and the electron bunch beams (Bahrdt, 1997). In the case of a large number of undulator periods, the Gaussian approximation on the photon beam is obtained by comparison with the angular distribution of intensity (a sinc function) (Lindberg & Kim, 2015). The approximation facilitates the convolution process, because of the Gaussian distribution of the electron beam in a storage ring, and gives a simplified expression of the brilliance. The Gaussian approximation, however, is not appropriate for the case of segmented undulators in a double mini-β function lattice, due to interference effects of the SR generated in each segment. The angular distribution of intensity generated by an electron passing through segmented undulators depends on the incident position and angle of the electron, corresponding to different optical phases. A non-Gaussian profile is therefore needed to evaluate the brilliance of a segmented undulator. However, it should also be noted that the non-Gaussian profile is important if the electron emittance is comparable with the wavelength of the photon beam.

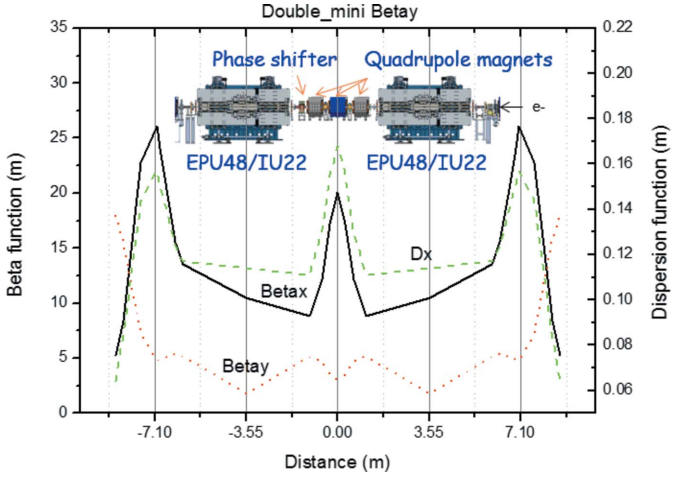

Figure 1
Beta (β) and dispersion (D) function as well as the location of IDs, quadrupole magnets and phase shifter (Chung *et al.*, 2017) in the double mini-β_y section.

The SR wave character becomes noticeable for small electron beam emittances, especially for a diffraction-limited light source. The SR properties in a low-emittance ring have therefore attracted many investigations (Geloni *et al.*, 2008; Bazarov, 2012; Tanaka, 2014). A typical method is to compute the WDF directly from the electron beam providing a general way to analyse the wave properties of SR without a Gaussian approximation (Kim, 1986). It is appropriate to evaluate the SR for segmented undulators. The on-axis WDF is chosen as the definition of the brilliance throughout this paper.

The transverse coherence photon flux of SR is enhanced with an increase of the SR brilliance. The coherent photon flux $F_{\rm coh}$ is therefore signified by the multiplication of the brilliance and the minimum value $\lambda^2/4$ of the phase space area in the transverse directions, where λ is the radiation wavelength (Kim, 1989). To be specific, $F_{\rm coh}$ as well as the degree of coherence in segmented undulator radiation must be evaluated by considering interference effects.

A typical method to determine the degree of coherence of the SR is to integrate the flux over a coherent area defined by the van Cittert–Zernike (VCZ) theorem. However, the VCZ theorem was studied and proved to be unsuitable in the near diffraction-limited region (Geloni *et al.*, 2008). Specifically, the VCZ theorem can be applied to analyse the coherent properties of quasi-homogeneous light, such as thermal light, but not to SR from third-generation light sources with a very small emittance in the vertical direction. The condition of the homogeneity in statistical optics means that the intensity distribution of the light source varies slowly compared with the width of the coherence (Goodman, 2015). The SR intensity distribution of the light source can be described by the electron beam size $\sigma_{x/y}$ in the horizontal and vertical direction. The coherent length is determined by the angular divergence of the electron beam $\sigma_{x'/y'}$ and given by $\lambda/(2\sigma_{x'/y'})$, which can be evaluated from equalizing the phase term of the electric field in equation (30) of Geloni *et al.* (2008) to be $\lambda/2$. The quasi-homogeneous condition for a suitable application of the VCZ theorem is therefore the electron beam emittance $\varepsilon_{x/y} > \lambda/2$. In the case of the Taiwan Photon Source (TPS) (energy and natural emittance are 3 GeV and 1.6 nm rad, respectively), the vertical emittance ε_y is around 1.6 pm rad, for a coupling constant of 0.001. The homogeneous condition is valid only if the photon energy is higher than 400 keV. To investigate the coherent properties of the desired photon energy at 0.4–20 keV, the direct integral of the cross-spectral density (CSD)

is used to determine the overall degree of coherence instead of applying the VCZ theorem in this work.

Typical methods to determine the brilliance (Wiedemann, 2007) and transverse coherence properties (*i.e.* the VCZ theorem) for segmented undulator radiation are incorrect. The magnets between segments, *e.g.* quadrupoles and phase shifter, change the focus of the electron beam as well as the trajectories of all electrons, leading to an overburdened evaluation. In this work, numerical analyses were performed to show a complete investigation on both properties for two arrangements, *i.e.* single and segmented undulators. We organize the paper as follows. In Section 2, the theoretical background for undulator radiation is given. It includes a review and discussion on the definition and properties of WDF and transverse coherence. The corresponding issues of a segmented undulator are then given in Section 3. Several practical issues such as the effects of phase shifter and quadrupoles are discussed. In Section 4, numerical results for the brilliance and transverse coherence in segmented undulator radiation at the TPS are shown. In Section 5, we discuss two issues affecting SR from the virtual source point to the endstation, *i.e.* electron beam displacement and focusing the beam at the sample point. The conclusion is given in Section 6.

2. Theoretical background of undulator radiation

The WDF was invented by Wigner (Wigner, 1932) to deal with a quantum-mechanics-based thermodynamic problem. Walther noticed the relation between the WDF and the radiance and coherence properties of optics (Walther, 1968). Then the concept of WDF was introduced by Coisson & Walker (1985) and Kim (1986) to the SR community about thirty years ago and is based on a phase-space method in wave optics. It follows the same transport rule as the geometrical optics and contains all the information of second-order correlation of the electric field. The WDF is indeed a four-dimensional distribution which cannot be plotted on paper or on a computer screen. But the two-dimensional projection of it provides a visual way to deal with the distribution of light in phase space although it is not a real photon distribution in phase space as in geometrical optics. The on-axis WDF contains information on the transverse coherence of two points placed symmetrically about the optical axis (Lindberg & Kim, 2015). However, the use of two-dimensional apertures to define the photon flux with coherent features is what the user needs. So, a reasonable parameter to define photon beam coherence should contain all information in the two-dimensional area. Although the on-axis WDF contains coherent information for a two-dimensional region, it still does not contain all coherent information because the information contained therein is only from symmetrically placed pairs of points. So, it is not easy to obtain the overall degree of coherence by using the WDF. For simplicity, the root-mean square of the degree of coherence is calculated by integrating the cross-spectral density in the whole area of the aperture. Note that the coherent flux that passes through the aperture is in general not equal to the well known definition of coherent flux ($F_{\rm coh}$) that is the multiplication of brilliance (B) and minimum phase space volume ($\lambda^2/4$) (Kim, 1989).

2.1. Wigner distribution function for brilliance

The Wigner distribution function for SR is defined by (Coisson & Walker, 1986; Kim, 1986)

$$\begin{aligned} W(\mathbf{r},\boldsymbol{\theta};\boldsymbol{\omega}) &= \left(\frac{1}{\lambda}\right)^2 \int \left\langle E\left(\mathbf{r}-\frac{\mathbf{r}'}{2};\boldsymbol{\omega}\right) E^*\left(\mathbf{r}+\frac{\mathbf{r}'}{2};\boldsymbol{\omega}\right)\right\rangle \\ &\quad \times \exp(-ik\mathbf{r}'\cdot\boldsymbol{\theta})\,\mathrm{d}^2\mathbf{r}' \\ &= \left(\frac{1}{\lambda}\right)^2 \int \left\langle \boldsymbol{\varepsilon}\left(\boldsymbol{\theta}-\frac{\boldsymbol{\theta}'}{2};\boldsymbol{\omega}\right) \boldsymbol{\varepsilon}^*\left(\boldsymbol{\theta}+\frac{\boldsymbol{\theta}'}{2};\boldsymbol{\omega}\right)\right\rangle \\ &\quad \times \exp\left(ik\mathbf{r}\cdot\boldsymbol{\theta}'\right)\mathrm{d}^2\boldsymbol{\theta}', \end{aligned} \tag{1}$$

where $\mathbf{r}=(x,y)$ defines the coordinates in any transverse plane and $\boldsymbol{\theta}=(\theta_x,\theta_y)$ is the angle coordinate between observer and undulator axis, E and ε are the position and angular representation of the electric field in the frequency domain, respectively, k and λ are the corresponding wavenumber and wavelength, respectively. The angle brackets represent the ensemble average (incoherent summation) of the radiation that is generated by all electrons in the beam. Since the electron bunch length is much longer than the wavelength of interest and there is no microbunch structure in the TPS, the WDF of the electron beam is treated as an incoherent summation of the radiation from each electron as described by Geloni *et al.* (2015) and Bazarov (2012).

Several possible definitions of the brilliance through the WDF were discussed by Bazarov (2012) and the authors chose the on-axis WDF $W(0,0)$ as the definition of the brilliance in their paper, that is

$$\begin{aligned} W(0,0) &= \left(\frac{1}{\lambda}\right)^2 \int \left\langle E\left(-\frac{\mathbf{r}'}{2}\right) E^*\left(\frac{\mathbf{r}'}{2}\right)\right\rangle \mathrm{d}^2\mathbf{r}' \\ &= \left(\frac{1}{\lambda}\right)^2 \int \left\langle \boldsymbol{\varepsilon}\left(-\frac{\boldsymbol{\theta}'}{2}\right) \boldsymbol{\varepsilon}^*\left(\frac{\boldsymbol{\theta}'}{2}\right)\right\rangle \mathrm{d}^2\boldsymbol{\theta}', \end{aligned} \tag{2}$$

which is, in general, the maximum value of the WDF for on-axis undulator radiation thereby also satisfying the definition given by Geloni *et al.* (2015). The physical meaning of brilliance can be regarded as the maximum concentration of the photon flux, as discussed by Geloni *et al.* (2015). In addition, in the limit of geometric optics (the emittance of the electron beam is much larger than the diffraction-limited photon beam emittance), this definition of brilliance is the maximum photon flux in the defined phase space (Geloni *et al.*, 2015).

The distribution of flux density $\mathcal{B}_x$ and $\mathcal{B}_y$ in the transverse phase space could be obtained by projecting the four-dimensional WDF on the $x-\theta_x$ or $y-\theta_y$ planes (Bazarov, 2012),

$$\begin{aligned} \mathcal{B}_x(x,\theta_x) &= \iint W(\mathbf{r},\boldsymbol{\theta})\,\mathrm{d}y\,\mathrm{d}\theta_y, \\ \mathcal{B}_y(y,\theta_y) &= \iint W(\mathbf{r},\boldsymbol{\theta})\,\mathrm{d}x\,\mathrm{d}\theta_x. \end{aligned} \tag{3}$$

These equations can be solved in a simplified form (Bazarov, 2012) by

$$\mathcal{B}_x(x,\theta_x)=\frac{1}{\lambda}\int\left[\int\left\langle E\left(x-\frac{x'}{2},y\right)E^*\left(x+\frac{x'}{2},y\right)\right\rangle \mathrm{d}y\right]\times\exp(ikx'\theta_x)\,\mathrm{d}x',$$
$$\mathcal{B}_y(y,\theta_y)=\frac{1}{\lambda}\int\left[\int\left\langle E\left(x,y-\frac{y'}{2}\right)E^*\left(x,y+\frac{y'}{2}\right)\right\rangle \mathrm{d}x\right]\times\exp\left(iky'\theta_y\right)\mathrm{d}y'. \quad (4)$$

As an example, a three-dimensional and contour map of the WDF-$\mathcal{B}_x$ for undulator radiation is shown in Fig. 2. In the contour map of Fig. 2, the electric field $\boldsymbol{\varepsilon}_k$ of the first harmonic of EPU48 radiation can be obtained (Lindberg & Kim, 2015) from equation (5) at the mid-point of the EPU48. The EPU48 is an elliptically polarizing undulator whose period length is 48 mm. Another undulator that will be discussed in this paper is the in-vacuum undulator IU22 whose period length is 22 mm. Both the EPU48 and IU22 are operated in horizontal linear mode throughout this paper,

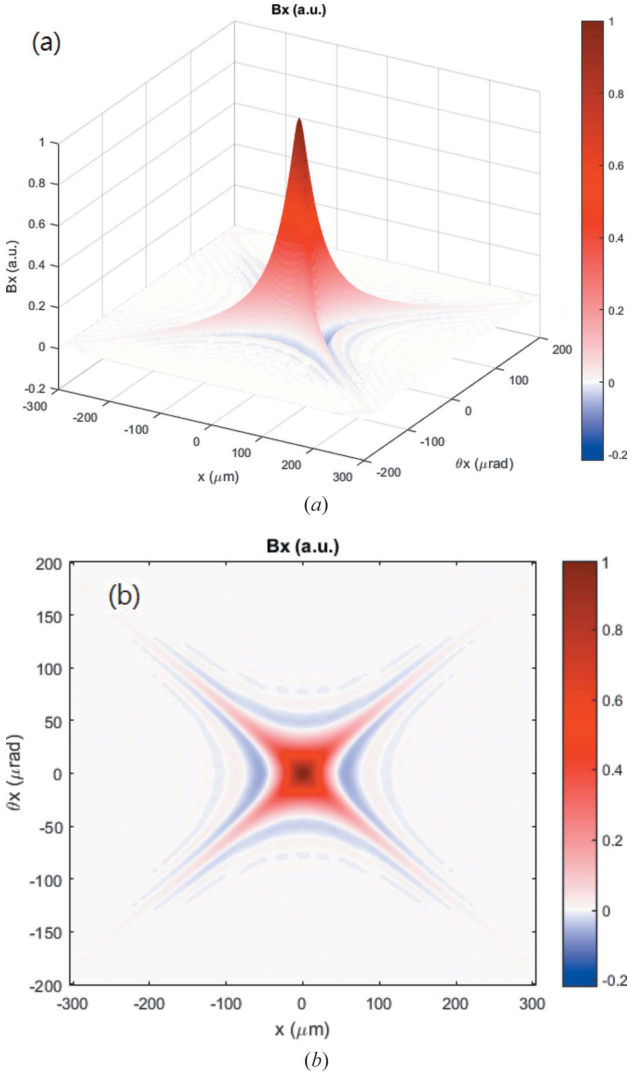

Figure 2
Normalized single electron intensity in a two-dimensional projection of the radiation WDF from a single EPU48 undulator (photon energy at 220 eV). (*a*) 3D graph, (*b*) contour map.

$$\boldsymbol{\varepsilon}_k(\boldsymbol{\theta};z=0)=\frac{eK[JJ]L_u}{8\pi\varepsilon_0\gamma c\lambda^2}\exp\left(-i\pi N_u\frac{k-k_r}{k_r}\right)\times\mathrm{sinc}\left[\pi N_u\left(\frac{k_r}{2k_u}\boldsymbol{\theta}^2+\frac{k-k_r}{k_r}\right)\right], \quad (5)$$

where $[JJ]=J_0[K^2/(4+2K^2)]-J_1[K^2/(4+2K^2)]$, $k_r=2\pi/\lambda_r$, $\lambda_r=(\lambda_u/2\gamma^2)[1+(K^2/2)]$, k_r is the wavenumber at resonant energy, and N_u, λ_r, K and λ_u are the period number, resonant wavelength, deflection parameter of the undulator and period length, respectively. The paraxial equation of the electric field $\boldsymbol{\varepsilon}_k(\boldsymbol{\theta};z=0)$ with non-zero initial coordinates of electrons $(\mathbf{x}_j,\mathbf{x}_j',\eta_j,t_j)$ is expressed by equation (6) (Lindberg & Kim, 2015). The terms $\mathbf{x}_j$, $\mathbf{x}_j'$, η_j and t_j represent the position, angle, energy deviation and time shift, respectively. η_j is not directly shown in equations (5) and (6) but it changes the γ term to $\gamma(1+\eta_j)$ in the wavenumber at resonant energy in equation (5),

$$\boldsymbol{\varepsilon}_k(\boldsymbol{\theta};\,z=0)=\exp(i\omega t_j)\exp(ik\boldsymbol{\theta}\cdot\mathbf{x}_j)\boldsymbol{\varepsilon}_k(\boldsymbol{\theta}-\mathbf{x}_j';\,z=0). \quad (6)$$

For high odd harmonic radiation, the profile of the radiation electric field $\boldsymbol{\varepsilon}(\theta_x,\theta_y)$ (that is the angular terms of the sinc-function) should be modified by Bessel's functions if the number of undulator periods is not large. For the IU22 at TPS, in our experience, the term $[JJ]\,\mathrm{sinc}\{\pi N_u[(k_r/2k_u)\boldsymbol{\theta}^2+(k-k_r)/k_r]\}$ is needed to be modified for the equation of reference (Wiedemann, 2007) with the replacement of $\theta\cos\varphi$ with θ_x and omission of the $\gamma^2\theta^2$ terms. The resulting modified equation is

$$\boldsymbol{\varepsilon}(\theta_x,\theta_y)\propto\Big\{J_{(3-h)/2}(C_1)\left[J_4(C_2\theta_x)+J_2(C_2\theta_x)\right]+J_{(1-h)/2}(C_1)\left[J_2(C_2\theta_x)+J_0(C_2\theta_x)\right]+J_{(-1-h)/2}(C_1)\left[J_0(C_2\theta_x)+J_{-2}(C_2\theta_x)\right]\Big\}\times\mathrm{sinc}\left[C_3\left(\theta_x^2+\theta_y^2\right)\right], \quad (7)$$

where $C_1=h[K^2/(4+2K^2)]$, $C_2=h[2K\gamma/(1+K^2/2)]$, $C_3=\pi N_u(k_r/2k_u)$ and h is the harmonic number. The electric field in the modified equation [equation (7)] was used to calculate the brilliance for comparison with *SPECTRA* results (Tanaka & Kitamura, 2001) to make sure that this formula is avaliable.

2.2. Overall degree of coherence

The cross spectral density Γ with contributions from any two points on a transverse plane with longitudinal coordinate z is defined as (Mandel & Wolf, 1995)

$$\Gamma(\mathbf{x}_1,\mathbf{x}_2;z)=\left\langle\mathbf{E}(\mathbf{x}_1)\,\mathbf{E}^*(\mathbf{x}_2)\right\rangle. \quad (8)$$

The angle brackets show the ensemble average of the radiation from the entire electron beam. The degree of coherence is $0\le|\gamma_{12}(\mathbf{x}_1,\mathbf{x}_2;z)|\le1$ with

$$\gamma_{12}(\mathbf{x}_1,\mathbf{x}_2;z)=\frac{\Gamma(\mathbf{x}_1,\mathbf{x}_2;z)}{\left[I(\mathbf{x}_1;z)\right]^{1/2}\left[I(\mathbf{x}_2;z)\right]^{1/2}}, \quad (9)$$

where I is the intensity. The degree of coherence is directly related to the visibility V of interference fringes in Young's interference experiment (Geloni *et al.*, 2008) in equation (10),

$$V = \frac{2\left[I(\mathbf{x}_1; z)\right]^{1/2}\left[I(\mathbf{x}_2; z)\right]^{1/2}}{I(\mathbf{x}_1; z) + I(\mathbf{x}_2; z)}\,\gamma(\mathbf{x}_1, \mathbf{x}_2). \tag{10}$$

For a finite radiation distribution, the overall degree of coherence γ (Luis, 2007) or the coherence mode purity is obtained by integrating the product of intensity and degree of coherence from the entire photon source size,

$$\gamma = \left\{\frac{\int I(\mathbf{x}_1; z) I(\mathbf{x}_2; z)\,\gamma_{12}^2(\mathbf{x}_1, \mathbf{x}_2; z)\,\mathrm{d}\mathbf{x}_1\,\mathrm{d}\mathbf{x}_2}{\left[\int I(\mathbf{r})\,\mathrm{d}\mathbf{r}\right]^2}\right\}^{1/2} = \left\{\frac{\int W^2(\mathbf{r}, \boldsymbol{\varphi})\,\mathrm{d}\mathbf{r}\,\mathrm{d}\boldsymbol{\varphi}}{\left[\int W(\mathbf{r}, \boldsymbol{\varphi})\,\mathrm{d}\mathbf{r}\,\mathrm{d}\boldsymbol{\varphi}\right]^2}\right\}^{1/2}, \tag{11}$$

where γ is the root-mean-square value of the degree of coherence by integrating any two-point pairs over the whole aperture region. As the radiation passes through an ideal aperture, the electric field is set to zero outside the aperture. Then γ presents the averaged coherence information of the photon flux that passes through the aperture to reach the experimental sample.

The well known VCZ theorem is usually used to estimate the coherent area (the size of the aperture) of SR and thus the coherent photon flux. However, it is invalid in the near-diffraction-limited region due to the non-homogeneous coherence feature of the undulator radiation (Geloni *et al.*, 2008). In fact, the derivation of the VCZ theorem is based on the assumption of an incoherent source (Mandel & Wolf, 1995). Instead, the degree of coherence in this work is obtained by direct calculation of the cross-spectral density based on the Monte Carlo method. To compare the coherent performance of different configurations of the undulator in different lattices, the coherent flux is the photon flux through an aperture which is defined by equation (12), the so-called coherent length $l_{cx,y}$,

$$l_{cx,y} = \frac{\lambda z}{4\pi\Sigma_{x,y}}, \tag{12}$$

where $\Sigma_{x,y}$ and λz are the effective source size and the photon wavelength, respectively, and

$$\Sigma_x = \left(\sigma_x^2 + \sigma_r^2\right)^{1/2}, \qquad \Sigma_y = \left(\sigma_y^2 + \sigma_r^2\right)^{1/2}. \tag{13}$$

Here, σ_r means the size of the photon beam of a single electron. For simplicity, equation (12) is still based on the VCZ theorem following the design report for the TPS beamline (Huang *et al.*, 2015). However, the degree of coherence for each possible configuration is not exactly the same since the aperture size which is defined by the VCZ theorem is indeed unavailable and the coherence properties are different for each configuration. To avoid a biased comparison between single and double undulator radiation, we need to check the difference of the overall degree of coherence to make sure that the degrees of coherence are close to each other for each configuration.

3. Issues of a tandem undulator

Quadrupoles between two collinear undulators focus off-axis electrons and thus change the electron path lengths passing the two midpoints of each undulator as shown in Fig. 3. This effect, which depends on the initial conditions of the electron trajectory at the entrance of the upstream undulator, will result in a phase difference between the two radiation beams that are generated in each of the undulators. In addition, a phase shifter is installed between two undulators to tune the path length difference. Another issue is the fraction of electrons that effectively contribute to the brilliance [this is somewhat related to the core emittance as discussed by Bazarov (2012)]. For a single undulator, the on-axis brilliance is calculated by the convolution of the WDF of the radiation generated by a single electron and the electron beam distribution in phase space. The calculation method of the WDF for a tandem undulator in a double mini-β_y lattice is different from that of a single undulator. In the simulation of a tandem

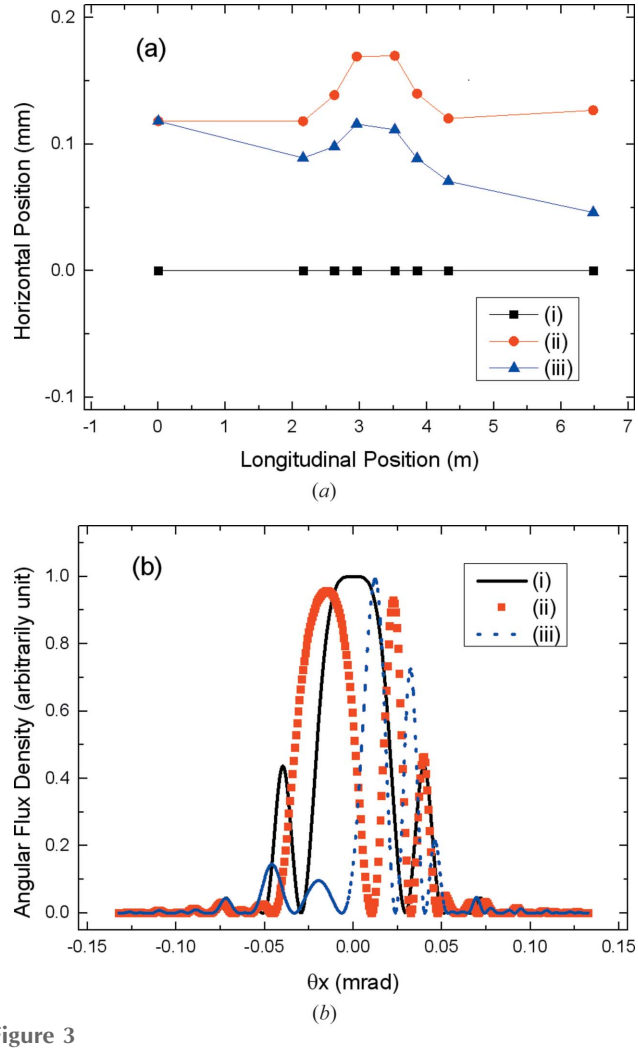

Figure 3
(*a*) Different electron trajectories in the straight section. (*b*) The corresponding angular flux density in different trajectories of (*a*). The three trajectories in (*a*) and (*b*) are: (i) on-axis electron, (ii) off-axis electron without angle deviation, (iii) off-axis electron with angle deviation.

undulator, the trajectories of each electron need to be calculated to know the phase difference of the radiation from two undulators since the quadrupole magnets change the path length difference. In addition, the radiation from two undulators needs to be propagated to the same transverse plane to obtain the total radiation field. These processes do not exist in the calculation of the radiation properties of a single undulator.

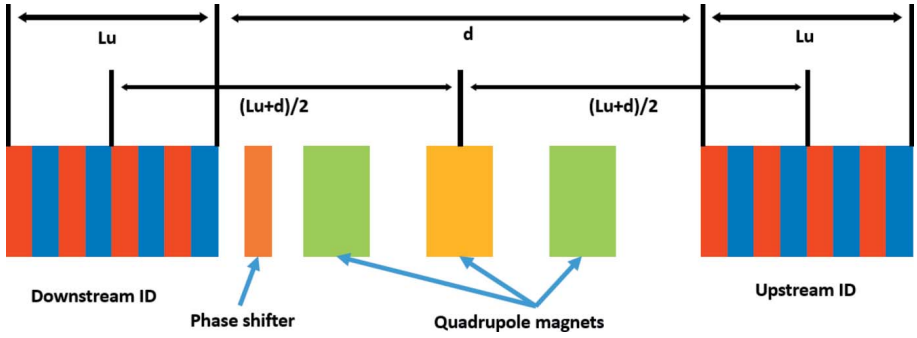

Figure 4
Configuration and relative location of the tandem undulators in the double mini-β_y lattice structure.

3.1. Phase shifter effect

An electron beam with zero emittance and energy spread is used to determine the effect of the phase shifter in a double undulator structure. To calculate the electric field $\boldsymbol{\varepsilon}$ of a segmented undulator ($\boldsymbol{\varepsilon}_{\rm total}$), the Fresnel diffraction formula equation (14) (Kim, 1986) is used to propagate the radiation field from a virtual source point in each undulator to a common transverse plane (*e.g.* midpoint between two undulators),

$$\boldsymbol{\varepsilon}_k(\boldsymbol{\theta}; z+l) = \exp\left[ikl\left(1-\boldsymbol{\theta}^2/2\right)\right]\boldsymbol{\varepsilon}_k(\boldsymbol{\theta}; z), \tag{14}$$

$$\begin{aligned}\boldsymbol{\varepsilon}_{\rm total} = {} & \exp(i\omega t_1)\exp\left[ikl_1\left(1-\boldsymbol{\theta}^2/2\right)\right]\boldsymbol{\varepsilon}_1\left(\boldsymbol{\theta}; z_{\rm up}\right) \\ & + \exp(i\omega t_2)\exp\left[ikl_2\left(1-\boldsymbol{\theta}^2/2\right)\right]\boldsymbol{\varepsilon}_2(\boldsymbol{\theta}; z_{\rm down}),\end{aligned} \tag{15}$$

where $\boldsymbol{\varepsilon}_1(\boldsymbol{\theta}; z_{\rm up})$ and $\boldsymbol{\varepsilon}_2(\boldsymbol{\theta}; z_{\rm down})$ are the electric fields for each undulator [equation (6)] at their virtual source points $z_{\rm up/down}$ and $t_2 - t_1$ represents the time delay for the electron transport from the virtual source point in the upstream undulator to the downstream undulator. l_1 and l_2 are the distances from each virtual source point to the common transverse plane, and the diffraction formula is the propagation of the electric field in the angular space with paraxial approximation. It is the same as the integral of Fresnel diffraction in position space.

For example, we consider a single electron passing through the two undulators (each of length $L_{\rm u}$), the drift space (d) and a phase shifter (with phase ξ) between undulators as shown in Fig. 4. The total electric field is described by equation (16),

$$\begin{aligned}\boldsymbol{\varepsilon}_{\rm total}(\boldsymbol{\theta}) = {} & \exp[-i(\xi/2)]\exp\left\{ik\left[(L_{\rm u}+d)/2\right]\left(1-\boldsymbol{\theta}^2/2\right)\right\}\boldsymbol{\varepsilon}_1(\boldsymbol{\theta}) \\ & + \exp[i(\xi/2)]\exp\left\{-ik\left[(L_{\rm u}+d)/2\right]\left(1-\boldsymbol{\theta}^2/2\right)\right\}\boldsymbol{\varepsilon}_2(\boldsymbol{\theta}).\end{aligned} \tag{16}$$

Defining $\bar{\beta}c$ as the average longitudinal velocity of the electron in the undulator, then

$$t_2 - t_1 = \frac{L_u}{\bar{\beta}c} + \frac{d}{\beta c} + \frac{\xi}{\omega}, \tag{17}$$

where

$$\bar{\beta} = \beta\left(1 - \frac{K^2}{4\gamma^2}\right)^{1/2}. \tag{18}$$

For simplicity, the phase difference term $(L_u/\bar{\beta}c) + (d/\beta c)$, generated by the travel time of the electron, is merged into the phase ξ for every case throughout this paper. We substitute the electric field of each undulator ($\boldsymbol{\varepsilon}_1$ and $\boldsymbol{\varepsilon}_2$) by the same symbol $\boldsymbol{\varepsilon}$ as in

$$\begin{aligned}\boldsymbol{\varepsilon}(\boldsymbol{\theta}) &= \boldsymbol{\varepsilon}_1(\boldsymbol{\theta}) = \boldsymbol{\varepsilon}_2(\boldsymbol{\theta}) \\ &= C_4 L_{\rm u}\,\mathrm{sinc}\left[C_3\boldsymbol{\theta}^2\right] = C_4 L_{\rm u}\,\mathrm{sinc}\left[\frac{k_{\rm r}L_{\rm u}}{4}\boldsymbol{\theta}^2\right],\end{aligned} \tag{19}$$

where $C_4 = eK[JJ]/(8\pi\epsilon_0\gamma c\lambda^2)$. The total electric field becomes then

$$\boldsymbol{\varepsilon}_{\rm total}(\boldsymbol{\theta}) = 2\cos\left\{k_{\rm r}\left[\frac{(L_{\rm u}+d)}{2}\right]\left(1-\frac{\boldsymbol{\theta}^2}{2}\right) - \frac{\xi}{2}\right\}\boldsymbol{\varepsilon}(\boldsymbol{\theta}). \tag{20}$$

The brilliance from a single particle in a segmented undulator can be expressed by

$$W(0,0) = \left(\frac{1}{\lambda}\right)^2 \int \boldsymbol{\varepsilon}_{\rm total}\left(-\frac{\boldsymbol{\theta}'}{2}\right)\boldsymbol{\varepsilon}^*_{\rm total}\left(\frac{\boldsymbol{\theta}'}{2}\right)\mathrm{d}^2\boldsymbol{\theta}', \tag{21}$$

and its numerical brilliance results are shown in Fig. 5. The oscillation of the normalized brilliance depends on the phase difference which represents the variation of the total spectral flux at the observation point. The two-dimensional projection of WDF-$\mathcal{B}_x$ at the centre between the two undulators (*i.e.* at

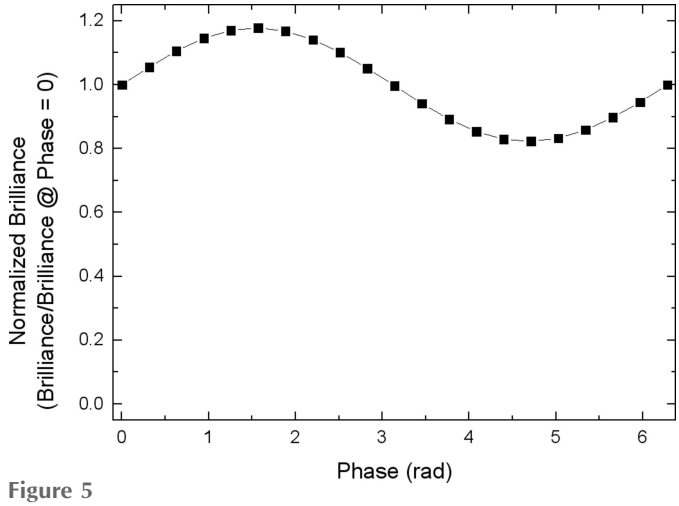

Figure 5
Normalized single particle brilliance (from double EPU48) as a function of phase difference (*i.e.* zero emittance and energy spread) at a photon energy of 220 eV.

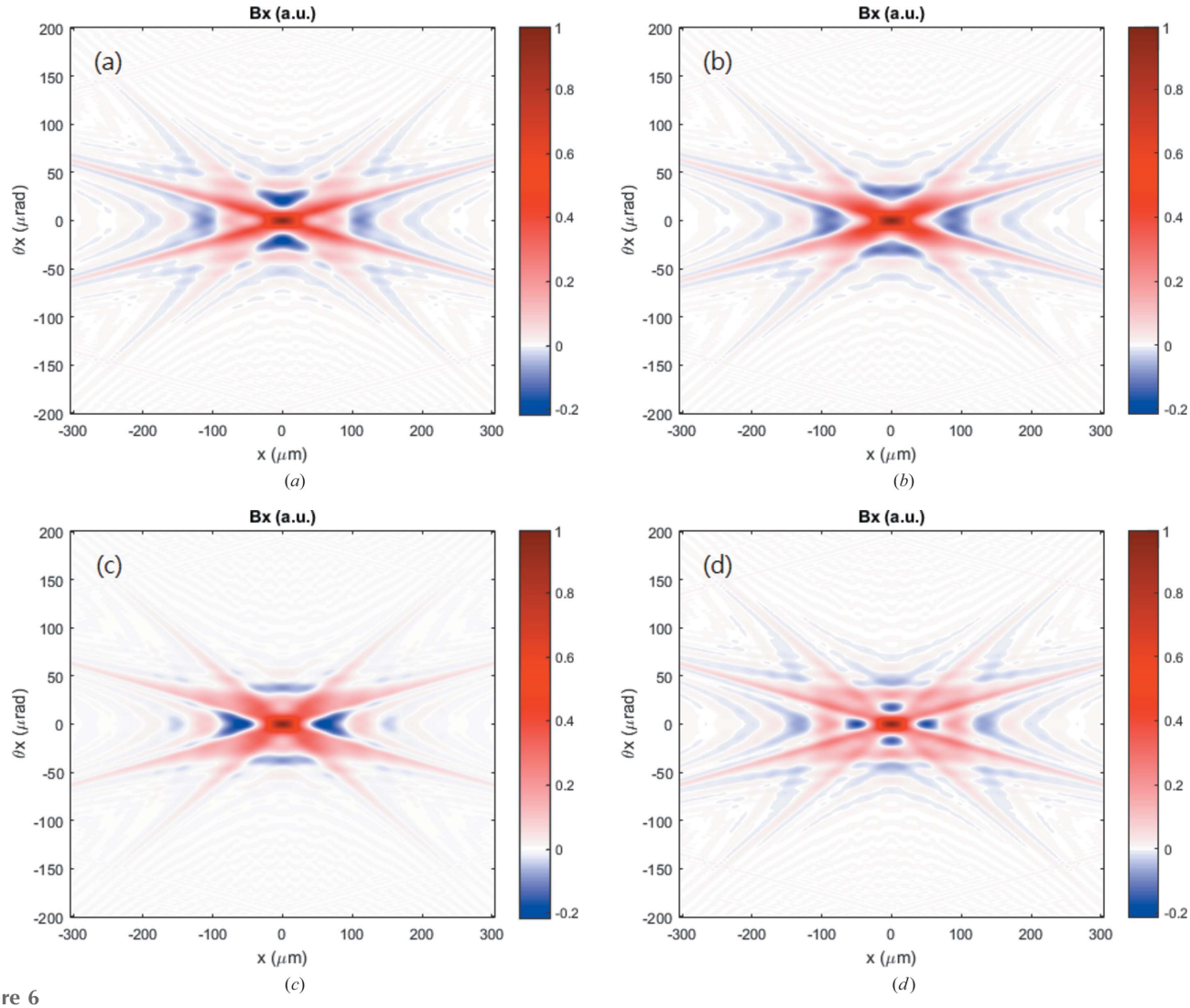

Figure 6
Intensity of the two-dimensional projection of the WDF in the tandem undulator onto the horizontal phase space. Panels (*a*), (*b*), (*c*) and (*d*) represent the phase shifter at 0, 0.5π, π and 1.5π, respectively.

the central quadrupole) from a single particle is plotted in Fig. 6.

3.2. Quadrupole magnet effect

The quadrupole magnets between two undulators kick the off-axis electrons and change their trajectories. The corresponding phase difference caused by the quadrupoles between the undulators due to the path length difference is

$$\Delta\varphi = kc\left(\frac{\Delta L_{\text{out of undulator}}}{\beta c} + \frac{\Delta L_{\text{in undulator}}}{\overline{\beta} c}\right), \qquad (22)$$

where $\Delta L_{\text{in/out of undulator}} = L_{\text{off-axis}} - L_{\text{on-axis}}$ is the path length difference of the off-axis and on-axis electron that is calculated in or out of the undulator. The phases of the off-axis electrons are the phase of the on-axis electron plus the result of equation (22). The relation of the phase difference between the off-axis electron and the on-axis electron to the electron position in phase space at the middle of the upstream undulator is plotted in Fig. 7. In this figure the vertical emittance and energy spread are assumed to be zero for simplicity. Once the position and velocity of an electron at the upstream undulator are known, the phase difference due to the quadrupole magnets can be obtained. The horizontal and vertical scales of Fig. 7 are $\pm\sigma_x$ and $\pm\sigma_{x'}$ of the horizontal electron beam size and angular divergence, respectively, at the upstream undulator in the double mini-β_y lattice. It seems that only a small fraction of electrons in the electron beam are in the in-phase region (white region in Fig. 7) in which the phase of the off-axis electron is close to that of the on-axis electron. So the phase relation between undulators cannot be preserved even for a soft X-ray (a few hundred eV) photon beam as shown in Fig. 7(*a*). But the above description of the phase relation for brilliance is not true. Only the paraxial electrons in the area of the wavelength in the horizontal phase space can effectively contribute to the on-axis Wigner function or brilliance, because the emittance of the photon beam of a single electron is at the scale of the wavelength. For 3 m EPU48 at

220 eV, the photon distributions in phase space are on the scales of σ_r = 15 μm and $\sigma_{r'}$ = 29 μrad, respectively, where $\sigma_{r'}$ is the angular divergence of the photon beam of a single electron. Comparing this photon distribution with the in-phase region in Fig. 7(*a*), it can be seen that most of the electrons that can effectively contribute to the brilliance are in the in-phase region; and the electrons with various phase differences outside the in-phase region do not contribute to the brilliance. The phase relation is therefore preserved for the brilliance of the soft X-ray photon beam under the influence of quadrupole magnets.

Fig. 7(*b*) shows that the higher the photon energy, the smaller the in-phase region in phase space. It seems that the interference effect should be less significant for a high-energy photon since fewer electrons preserve the phase relation.

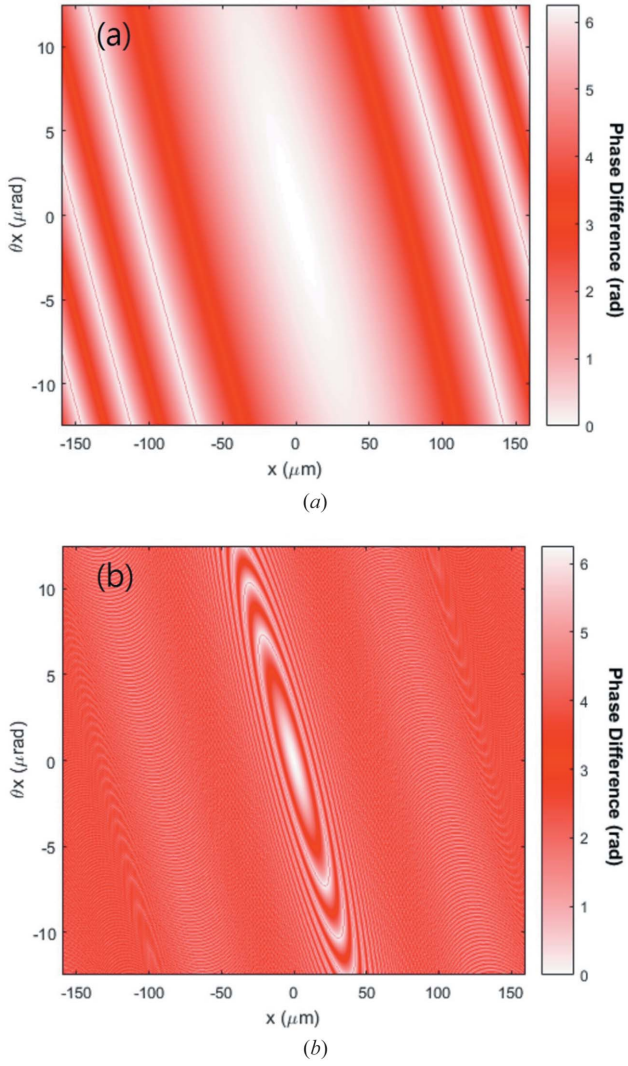

Figure 7
Phase difference induced by quadrupoles in the horizontal phase-space at the middle of the upstream undulator in the double mini-β_y lattice, (*a*) in the soft X-ray energy at 220 eV from an EPU48, (*b*) in the hard X-ray energy of 20 keV from an IU22. The horizontal and vertical scales of the figures are $\pm\sigma_x$ and $\pm\sigma_{x'}$ of the horizontal electron beam size and angular divergence, respectively. The vertical emittance and energy spread of the electron beam is zero.

However, the emittance of the photon beam of a single electron is inversely proportional to the photon energy. Therefore, the phase relation could be preserved for the hard X-ray photon beam (a few keV) if the reduction of the in-phase region is slower than the emittance of the photon beam as the photon beam increases. It turns out that, from numerical calculation, the in-phase region is also almost inversely proportional to the photon energy for the horizontal phase space of the double mini-β_y lattice in the TPS. As a result, the interference efficiency of double undulators on the brilliance is almost independent of the photon energy under the influence of quadrupole magnets, since the ratio of the in-phase region and the emittance of the photon beam is almost kept the same for different photon energies. Nevertheless, considering the contribution of the phase difference from the energy spread of the electron beam, the phase relation decreases as the photon energy increases. The energy spread changes the speed of each electron and causes a phase difference. This effect plays an important role when the photon energy is sufficiently high. For the TPS, the energy spread destroys the phase relation for a photon beam of energy a few keV.

3.3. Electron bunch effect on the on-axis WDF

There are two sources of brilliance gain from a tandem undulator in a double mini-β_y lattice. The first one is the amplitude of the electric field which determines the number of photons generated by a single electron being directly proportional to the total length of the undulator. The second one is the matching of the electron and photon beam in the two transverse phase spaces. Comparing Figs. 2(*b*) and 6(*c*) with the coherence relation, the angular divergence of the photon beam is smaller in the double undulator than in the single undulator configuration. This means that more electrons will contribute to the brilliance for a tandem undulator than a single undulator if $\sigma_x \gg \sigma_r$ and $\sigma_{r'} \gg \sigma_{x'}$. This conclusion also applies to single undulators of different lengths. If, on the other hand, two undulators are considered as two independent sources (*i.e.* incoherence relation), the phase-space matching will take place at the virtual source points of each undulator in the double mini-β_y lattice. In this case, the phase-space matching in the double mini-β_y lattice is more effective than for a single mini-β_y for $\sigma_y \gg \sigma_r$ and $\sigma_{r'} \gg \sigma_{y'}$. For these two reasons, the brilliance depends nonlinearly on the total length of the tandem undulator.

4. Numerical analysis results using WDF

In this section, the numerical analysis results of both brilliance and coherent photon flux are shown and discussed. In order to understand the effect on the brilliance and coherent photon flux due to emittance and energy spread in the tandem undulator, a Monte Carlo simulation with WDF is used. In the simulation, the initial transverse position, velocity and energy of electrons are generated by a Gaussian distribution with the standard values equal to the electron beam size, electron beam divergence and energy spread of the electron beam, respec-

tively, at the centre of the upstream undulator. The distribution in the transverse position–velocity phase space is an inclined Gaussian distribution according to the betatron function. Then the matrix method is used to calculate the trajectories of the electrons from the upstream to the downstream undulator without consideration of the focusing effect of the undulator. The lengths of the trajectories of the off-axis electrons are compared with those of the on-axis electrons to obtain the phase difference in equation (22). The electric field generated by two undulators is calculated by equations (5)–(7) and propagated through equation (14) to the centre of the straight section in order to calculate the brilliance. The propagated electric fields of each undulator are combined together to form the total electric field of the segmented undulator. To calculate the brilliance, the electric field of each electron is used to find the on-axis Wigner function [equation (2)] and sum up incoherently to obtain the on-axis brilliance of the electron beam. For the brilliance, about 250000 and 1000000 particles are tracked in the soft and hard X-ray regions, respectively. First, the numerical results of the normalized brilliance as a function of the phase delay of the phase shifter are shown in Fig. 8. Figs. 9 and 10 then show the brilliance for other possible undulator configurations of EPU48 and IU22 at the TPS that are listed in Table 1. Five configurations are studied to understand the characteristics of the brilliance and coherent flux: a single 3 m-long undulator in (i) a 7 m straight section (3M7MS), (ii) a 12 m straight section (3M12MS), and (iii) one 6 m-long undulator in a 12 m straight section (6M12MS), (iv) a 3 m-long undulator downstream of a

Table 1
Beam size and angular divergence of all possible configurations of EPU48 and IU22 at TPS.

	σ_x (μm)	$\sigma_{x'}$ (μrad)	σ_y (μm)	$\sigma_{y'}$ (μrad)
3 m ID in 7 m straight section (3M7MS)	121	17.2	1.61	0.99
3 m ID in 12 m straight section (3M12MS)	161	12.5	3.11	0.51
6 m ID in 12 m straight section (6M12MS)	161	12.5	3.11	0.51
3 m ID at downstream of double mini-β_y lattice (3MDMBYS)	165	12.7	1.67	0.96
3 m + 3 m IDs at double mini-β_y lattice (6MDMBYS)	165	12.7	1.67	0.96

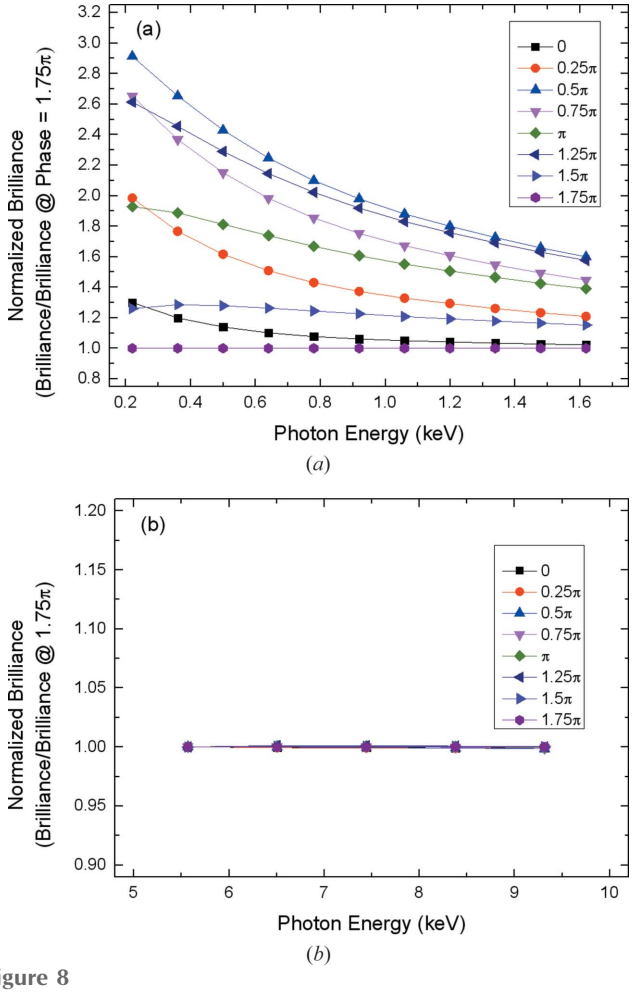

Figure 8
Brilliance as a function of phase difference in (*a*) the soft X-ray region radiated from a double EPU48 and (*b*) the hard X-ray region radiated from a double IU22.

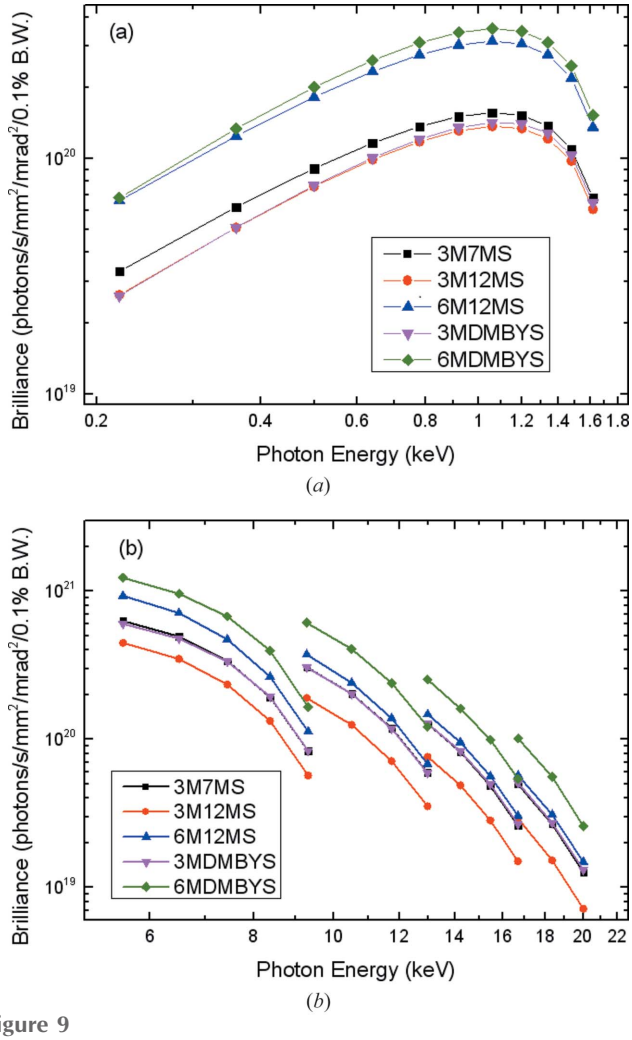

Figure 9
Brilliance comparison of possible undulator configurations in the TPS. (*a*) First harmonic energy of an EPU48, (*b*) third to ninth harmonics energy of IU22.

12 m double mini-β_y section (3MDMBYS) and finally (v) two 3 m-long undulators in a 12 m double mini-β_y section (6MDMBYS). The ratios of brilliance and photon flux for double and single undulators are calculated to see whether a double undulator can generate more brilliant light and provide more coherent flux than a single undulator. In all these configurations, the aperture size for the tandem undulators is chosen to be the same as the value for a single downstream undulator. For the numerical results of the brilliance, the effect of a phase shifter is significant and is more important in the soft X-ray than hard X-ray region as shown in Fig. 8. The brilliance can vary by 2.9 times the value of the different phase in the soft X-ray region but there is no difference in the hard X-ray region. This is due to more significant interference effects for the tandem undulator in the original phase space for soft X-rays which is not the case in the hard X-ray region.

4.1. Undulator configuration in the collinear case

Fig. 10 shows a comparison of the brilliance in the soft X-ray (220–1600 eV) and in the hard X-ray region (5.5–9.3 keV) for different undulator configurations. All brilliance values from different configurations are normalized to one 3 m undulator downstream of the double mini-β_y section (3MDMBYS). The vertical electron beam size and angular divergence of 3M7MS are close to those of 6MDMBYS and 3MDMBYS. Meanwhile, the horizontal electron beam size and angular divergence of 3M12MS are close to those of 6M12MS, 6MDMBYS and 3MDMBYS. It can be easily understood that the brilliance from 3M7MS is higher than that from 3M12MS and 3MDMBYS in the soft X-ray region. Meanwhile, the 3MDMBYS and 3M7MS brilliance values are higher than that from 3M12MS in the hard X-ray region. This is because in the soft X-ray region (*e.g.* σ_r and $\sigma_{r'}$ are 15 µm and 29 µrad at 220 eV) all 3 m undulator cases satisfy the relations $\sigma_x \gg \sigma_r$, $\sigma_{x'} \simeq \sigma_{r'}$, $\sigma_y \ll \sigma_r$ and $\sigma_{y'} \ll \sigma_{r'}$. The variations of σ_y and $\sigma_{y'}$ do not affect the brilliance significantly since the vertical size divergences are both dominated by the photon beam. The effect on brilliance from σ_x is direct, since it dominated the horizontal size, but not so for $\sigma_{x'}$, since $\sigma_{x'}$ does not dominate the horizontal divergence and is even smaller than $\sigma_{r'}$. The effect of decreasing σ_x is larger than that of increasing $\sigma_{x'}$. Considering that the product of σ_x and $\sigma_{x'}$ is almost constant for each configuration, it is better to have a small σ_x rather than a small $\sigma_{x'}$ in the soft X-ray region. On the other hand, the brilliances of 3MDMBYS and 3M7MS are higher than from 3M12MS in the hard X-ray region. For the hard X-ray region (*e.g.* σ_r and $\sigma_{r'}$ are 3 µm and 6 µrad at 5.5 keV), the beam size and angular divergence relations are $\sigma_x \gg \sigma_r$, $\sigma_{x'} > \sigma_{r'}$, $\sigma_y \simeq \sigma_r$ and $\sigma_{y'} < \sigma_{r'}$. The horizontal electron beam size and divergence are not important in terms of influencing the brilliance since both σ_x and $\sigma_{x'}$ are larger than σ_r and $\sigma_{r'}$, respectively. It is more important to have a small σ_y than a small $\sigma_{y'}$ because $\sigma_{r'}$ dominates the vertical divergence while neither σ_y nor σ_r dominate the vertical size.

Now, a comparison of the brilliance in the 12 m sections of 6M12MS, 3MDMBYS and 6MDMBYS is made and the results are shown in Fig. 10. The brilliance of 6MDMBYS is about 2.5 and 2 times higher compared with 3MDMBYS in the soft X-ray region and hard X-ray region, respectively. This result shows that an interference exists between the radiation pulses from the two undulators in the soft X-ray region but not in the hard X-ray region. The brilliance of 6MDMBYS is higher than that of 6M12MS. This is due to the fact that the phase-space matching between electron and photon beam in the vertical phase space is better for 6MDMBYS than for 6M12MS since σ_y is smaller in the former configuration, as described in Section 3.3.

Next, we consider the photon flux for the coherent radiation as requested from users in different configurations of the undulators. From Huang *et al.* (2015), the sample position is located 59 m away from the centre of the straight section and the aperture size (*i.e.* the coherence length) is determined by this distance. For 3MDMBYS, the longitudinal position z in equation (12) is chosen as 59 m minus the distance between the middle of the straight section and the middle of the downstream undulator, and the effective beam sizes $\Sigma_{x,y}$ are

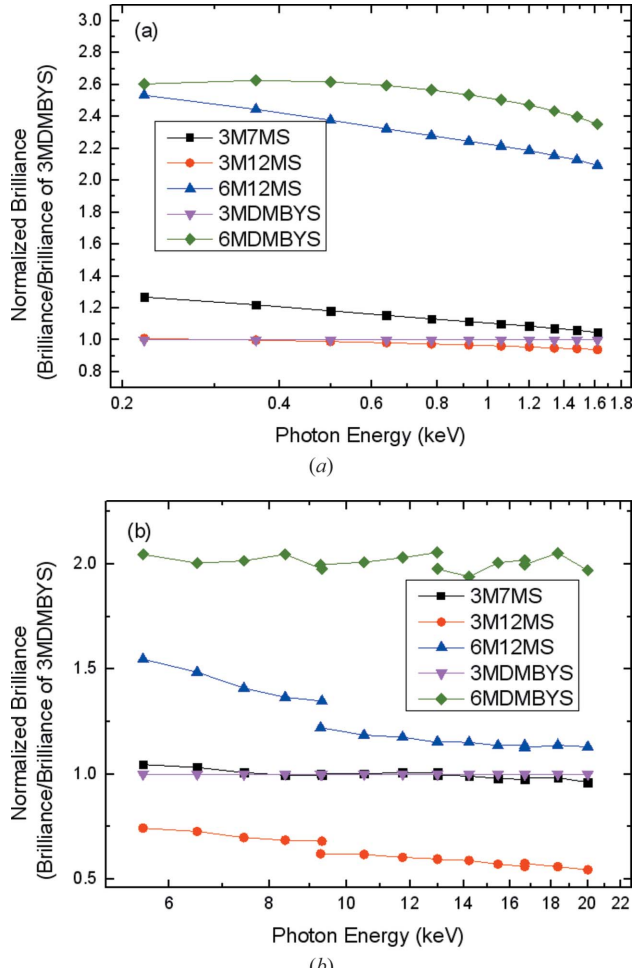

Figure 10
Normalized brilliance of possible undulator configurations at the TPS. (*a*) First harmonic energy of EPU48, (*b*) third to ninth harmonics energy of IU22.

the values at the virtual source point in the downstream undulator. For the case of 6MDMBYS, the coherent area (*i.e.* the aperture) is chosen to be the same as that of 3MDMBYS for simplicity. Unlike brilliance, the effect of the phase shifter on the coherent flux, shown in Fig. 11, is not significant even in the soft X-ray region. This is because more electrons contribute to the coherent photon flux than the brilliance. The coherent flux is defined as the photon flux that passes through the aperture. Since the aperture includes the optical axis, all the electrons that have a non-zero on-axis flux density contribute to the coherent flux. However, since the photon beam divergence is larger than the electron beam divergence in the horizontal axis for the soft X-ray region, the radiation from almost all the electrons would contribute to the on-axis flux density and thus to the coherent flux. The distribution of the electron beam is larger (especially in the horizontal size) than the in-phase region in Fig. 7(*a*), so the photon beam with any phase contributes to the coherent flux and thus the phase relation disappears. As a result, the interference between the upstream and downstream undulators almost disappears and the flux integration in the aperture region is the incoherent summation for each undulator. The incoherent summation of 6MDMBYS is not double that of 3MDMBYS but only about 1.8 times (see Figs. 12 and 13) due to the distance difference of the virtual source points in the upstream and downstream undulator to the aperture location in the case of 6MDMBYS. The ratio of the coherent flux between 3MDMBYS and 6MDMBYS could be tuned by using a focusing mirror in the beamline, but a more detailed treatment of this problem is not part of this paper.

These results show a different behaviour for brilliance and coherent flux for an electron beam of finite emittance and energy spread. In many articles (Bazarov, 2012; Thompson *et al.*, 2009) the coherent flux is directly proportional to the brilliance following Kim's equation (Kim, 1989),

$$F_{\rm coh} = B(\lambda/2)^2, \tag{23}$$

where B and $(\lambda/2)^2$ are the brilliance and minimum possible phase space area, respectively. The coherent flux is different for detailed photon flux calculation in the aperture area from the definition in equation (23). The coherent flux depends

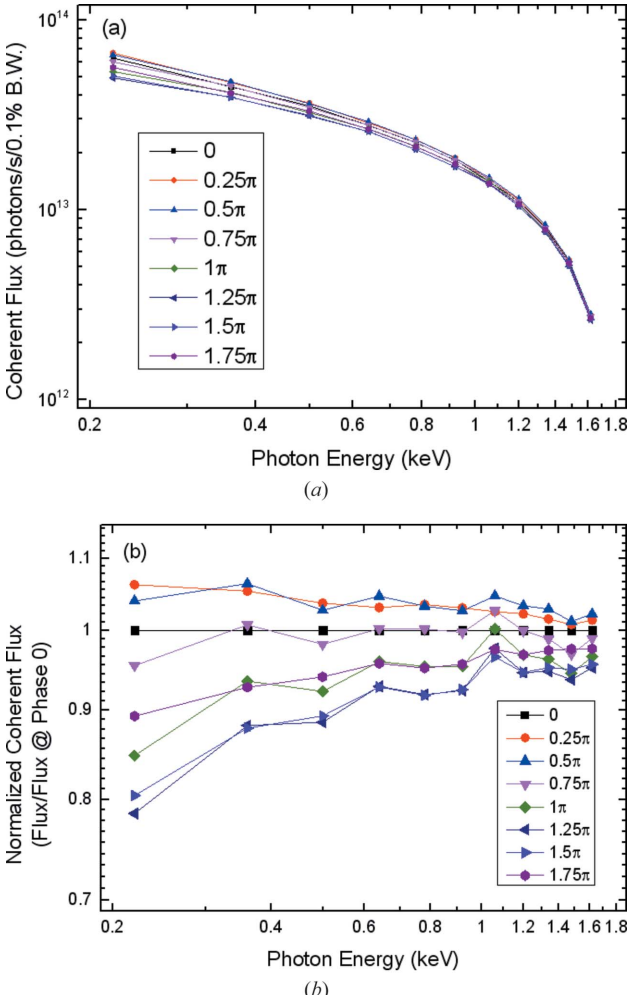

Figure 11
Integrated coherent flux in the aperture of EPU48 in horizontal linear mode in the double mini-β_y lattice for different phases. (*a*) Flux, (*b*) normalized flux.

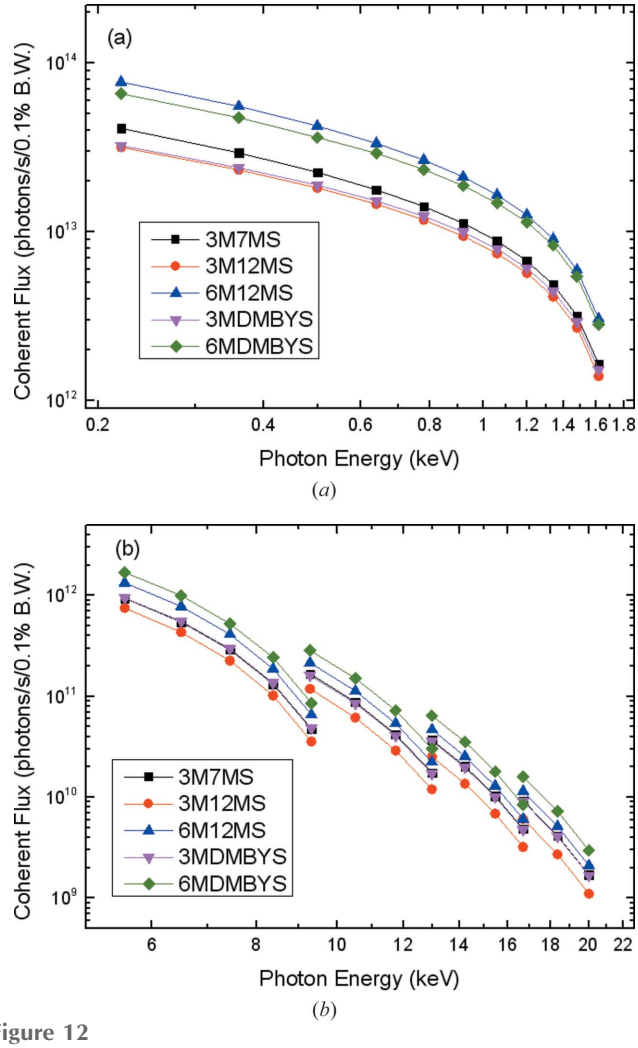

Figure 12
Integrated coherent flux inside the aperture for possible undulator configurations at the TPS. (*a*) Soft X-ray region and (*b*) hard X-ray region.

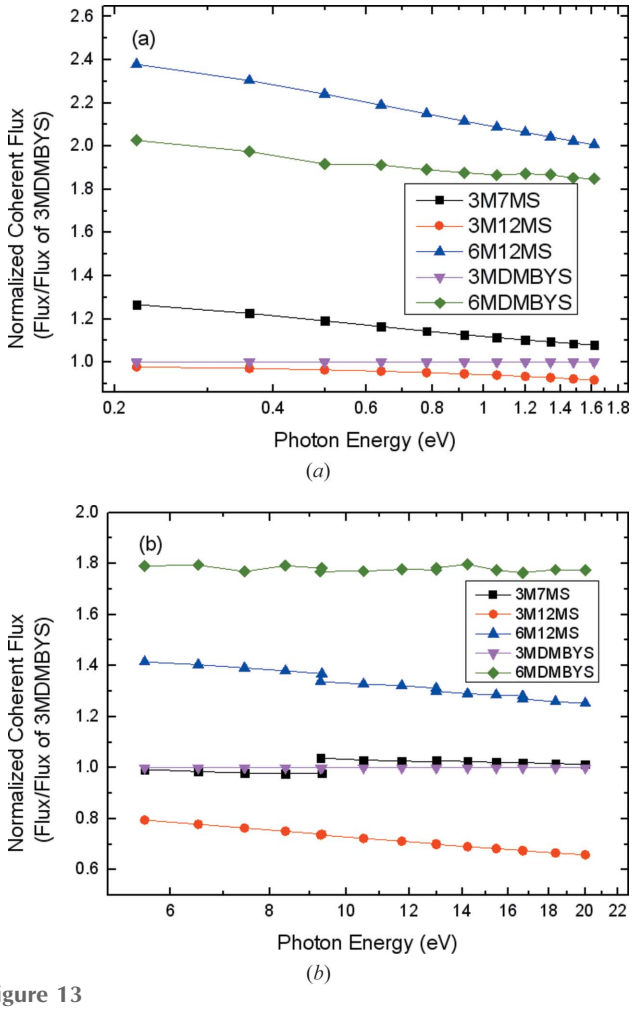

Figure 13
Normalized integrated coherent flux inside the aperture for possible configurations of undulators at the TPS. (*a*) Soft X-ray region and (*b*) hard X-ray region.

weakly on the phase shifter at any photon energy, but the brilliance is very sensitive to its settings in the soft X-ray region. However, as mentioned previously, the brilliance determines how well SR can be focused. Therefore, the phase shifter can be used to enhance the brilliance of the tandem undulator in the soft X-ray region.

4.2. Overall degree of coherence (ODOC) of the photon flux constraint in the aperture

The aperture size for collecting the coherent flux of a tandem undulator is set to be the same as that of a single downstream undulator. We have not discussed the behaviour of the ODOC in these configurations so far. Whether the ODOC will be decreased in our case of a double mini-β_y lattice should be checked by numerical methods that define the degree of coherence [equation (9)].

To calculate the ODOC of the electric field in the aperture area, a two-dimensional area with equal space is defined in the aperture plane. The ODOC is also obtained by a Monte Carlo based simulation for the degree of coherence of all pairs of elements of the area. In the simulation, the electric field of the segmented undulator is propagated to the aperture, *i.e.* 59 m away from the centre. A three-dimensional array of the electric field is generated, and each element E_{ijn} in the array represents the electric field that is contributed by the nth electron at a transverse position in the aperture corresponding to indices i and j for horizontal and vertical position, respectively. The cross spectral density of any two points in the aperture is the dot product of the corresponding vectors E_{ij} which contains the contribution of all the electrons at a transverse position. The dot products of all pairs of vectors E_{ij} in the array are summed up to obtain the numerator of equation (11) to obtain the ODOC. The result shows that there is no significant (at least lower than our simulation error) difference between 3MDMBYS and 6MDMBYS in both the soft and hard X-ray region. The ODOCs of IU22 at 9.3 keV for 3MDMBYS and 6MDMBYS are both around 0.97. This is due to the fact that the distance between two undulators is much smaller than the distance between the aperture and downstream undulator.

5. Electron deviation between the tandem undulator and focusing effect

The discussion in the previous section considered ideal cases where both undulators share the same optical axis. However, the electron beam position may deviate from the ideal orbit in practical cases. Therefore, the effects of the electron trajectory displacement are analysed by a two-dimensional projection of the WDF in phase space and the ODOC. The focusing problem for the photon flux passing through the aperture of the tandem undulator is described briefly in this section.

The deviation of the electron position in each undulator also affects the performance of the light source. Two examples are given to deal with this issue for both brilliance and coherent flux. We consider a simple example (Fig. 14) where the electron beam is displaced (without a kick angle) in the horizontal direction in the second undulator. If this beam displacement is larger than the size of the photon beam of the single electron, the brilliance is defined only by a single undulator. However, if the deviation is smaller than the

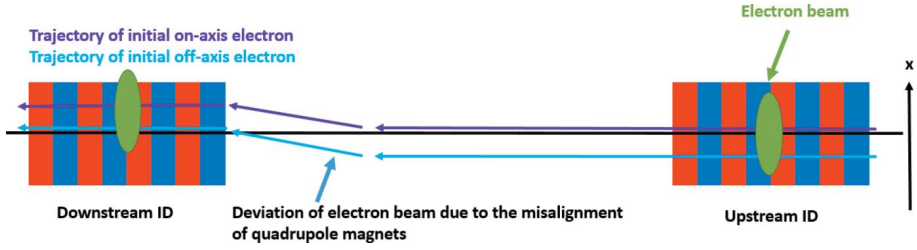

Figure 14
Electron bunch trajectory displacement and offset passing the downstream undulator in a double mini-β_y lattice.

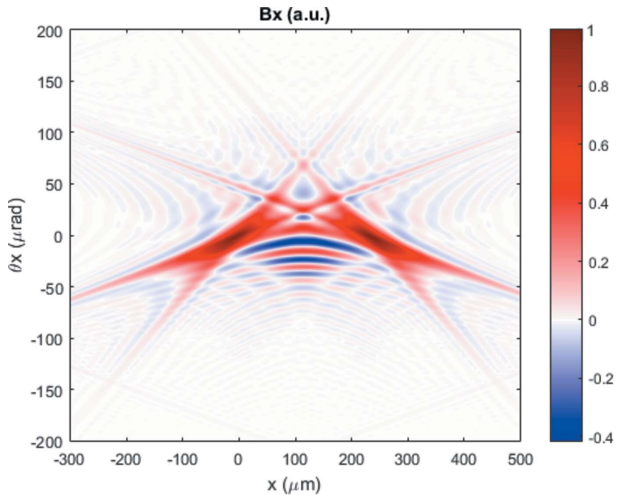

Figure 15
Intensity distribution of the two-dimensional projection of the WDF of the radiation from an electron bunch with a trajectory displacement and offset (see Fig. 14) in the downstream undulator of the double mini-β_y lattice. The undulator is EPU48 in horizontal linear mode.

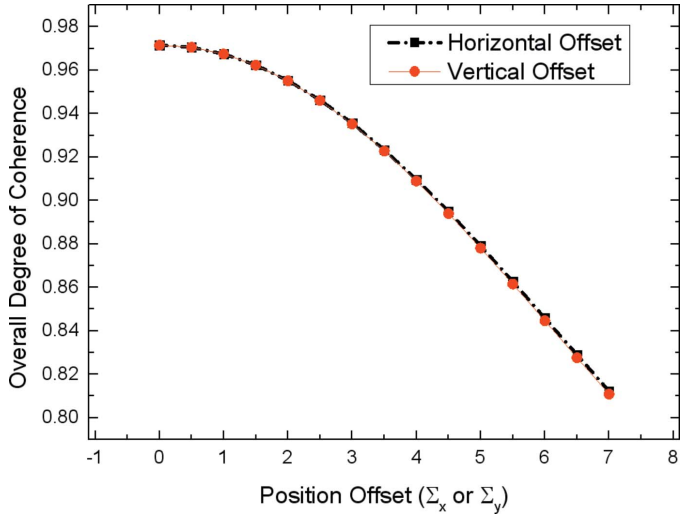

Figure 16
Variation of the ODOC with respect to orbit distortions in units of the effective horizontal and vertical beam size. The undulator is EPU48 in horizontal linear mode.

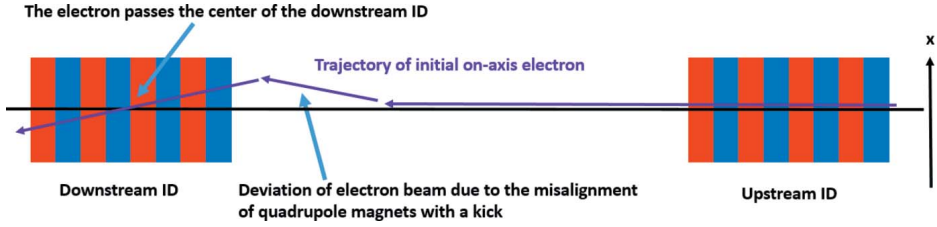

Figure 17
Electron trajectory with a kick angle in the downstream undulator of the double mini-β_y lattice.

electron beam size, there exist some electrons (the blue trajectory in Fig. 14) that pass through the upstream undulator that can also contribute to the photon coherence in the downstream undulator. These electrons contribute to the brilliance but there may be no interference at the origin of the phase space since the WDF of each electron in the two individual undulators are separated too far in phase space (see Fig. 15 at 220 eV) and the WDF of different electrons in the two undulators add incoherently. In this case, the phase shifter will be useless for brilliance. Next, the ODOC is calculated for different electron displacements at an energy of 9.3 keV and is shown in Fig. 16 for a tandem undulator as a function of the electron displacement. The electron displacement is measured in units of the effective source size $\Sigma_{x,y}$ for a single undulator. Fig. 16 shows that the ODOC is almost the same for displacements in both the horizontal and vertical plane. In order to maintain a reasonable and constant ODOC, the electron displacement should be well controlled within one unit of effective source size. It is much more difficult to keep the same ODOC in the vertical direction than in the horizontal since the coupling constant is very small and is less than 0.1%.

Here, we consider another case: Fig. 17 shows a case where the electron trajectory has an angle but still passes through the axis in the middle of the second undulator. Then the radiation generated in the second undulator may not contribute to the brilliance. The results can be seen in the contour map of the WDF in Fig. 18 which shows that the distributions of the two WDFs in phase space are separated. Unless the electron beam displacement and angle are both larger than the electron beam size and angular divergence, the brilliance from the second undulator will not be significantly reduced. However, the phase shifter has still no effect on the brilliance if there exists a kick angle larger than the photon angular divergence.

If the electron deviation is well controlled at the level of the effective beam size $\Sigma_{x,y}$ and divergence $\Sigma_{x',y'}$, the second undulator can contribute to the brilliance. The brilliance of a

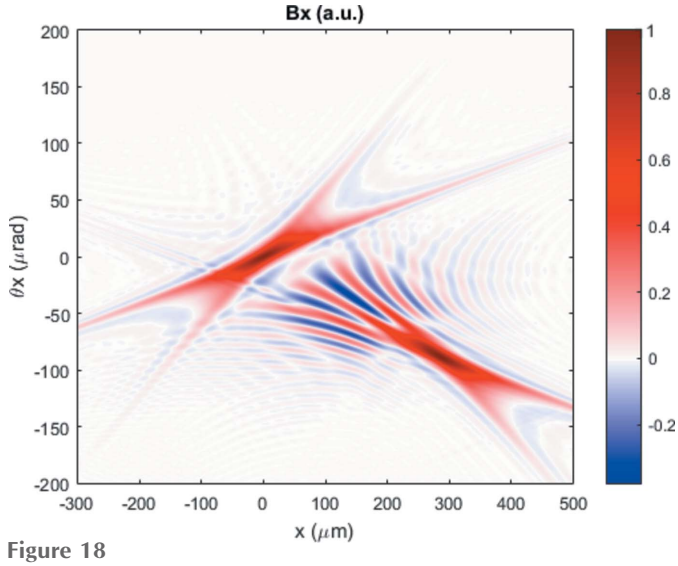

Figure 18
Two-dimensional projection of the radiation WDF from an electron beam with a kick angle in the downstream undulator of the double mini-β_y lattice (see Fig. 17). The undulator is EPU48 in horizontal linear mode.

double undulators is at least two times larger than from a single undulator. If the electron path distortion is much smaller than the photon beam size and divergence, then the photon phase relation between the two undulators will be preserved and the brilliance gain could be more than twofold. But this condition is difficult to satisfy in the hard X-ray region, since the electron path distortion needs to be controlled to less than a micrometre or microradian.

The photon flux radiated from the upstream and downstream undulator and passing the aperture can be considered as the incoherent summation of the photon flux. The tandem undulator can be considered as two independent sources at different longitudinal position. The focusing efficiency in the tandem undulator case will become worse, since the distance from the virtual source points of each undulator to the focusing elements are different. Therefore, the focal points for each undulator will be different. However, if the ODOC of the flux in the aperture is close to unity, the wavefront of the radiation from both undulators will be similar in the aperture and one focusing mirror behind the aperture can focus the radiation beam well in the tandem undulator structure. It could also be expected that the focusing efficiency decreases as the size of the aperture increases.

6. Conclusions

In this paper, wave optics based on the WDF method are used to analyse the performance of the tandem undulator in the double mini-β_y section in the TPS. The brilliance of a tandem undulator can be more than twice that of a single undulator in the soft X-ray region since the phase relations of paraxial electrons are preserved. However, the phase relation in the longitudinal axis cannot be kept in the hard X-ray region. Numerical results show that the brilliance is the summation of the incoherent flux of two undulators in the hard X-ray region. On the other hand, the phase relation is not important for obtaining the coherent flux that passes through the aperture defined in equation (12) even in the soft X-ray region.

Phase-space matching of the electron and the photon beam diffraction-limited emittance in each undulator plays an important role in the double mini-β_y lattice especially when the tandem undulator is considered as being two independent sources. The analysis show that the brilliance performance of the tandem undulator in the double mini-β_y section is superior to a single undulator with the same number of periods in a single mini-β_y section. In this case, the brilliance performance especially will be more obvious in the hard X-ray region.

The coherent flux calculation shows that the ODOC is the same for the single and the double undulator when the distance from the undulator to the aperture is much larger than the distance between the tandem undulators. Meanwhile, the coherent flux (*i.e.* the photon flux in the aperture) contribution from the upstream undulator of the tandem undulator is 80% of that of the downstream undulator, which could be improved by increasing the distance between the undulator and the aperture, or by focusing the two photon beams to the same spot size at the aperture location.

In summary, both brilliance and coherent flux can be enhanced by the second undulator of the tandem undulator at the TPS. To enhance the brilliance in the double mini-β_y lattice, the phase shifter is important in the soft X-ray region but is not necessary in the hard X-ray region. In addition, any electron displacement between the tandem undulators must be carefully controlled. For the coherent flux, the phase shifter is not important either in the soft X-ray or in the hard X-ray region. There are gains in brilliance and coherent flux in the TPS tandem undulator. However, there may not be a gain in other light source facilities depending on the accelerator lattice design and undulator parameters. The phase relation between undulators and phase-space matching of each undulator should be carefully evaluated while any transverse electron beam displacement needs to be taken into account to evaluate the gain performance.

Acknowledgements

The authors would like to thank Professor Helmut Wiedemann for providing good comments and correcting this article. The authors also thank Ms S. T. Chang for her opinions on programming computer code. NSRRC staff members Dr M. S. Chiu and Dr C. C. Kuo are commended for their TPS double mini-β_y lattice assistance.

Funding information

The following funding is acknowledged: Ministry of Science and Technology of Taiwan (contract No. MOST 106-2112-M-213-004).

References

Bahrdt, J. (1997). *Appl. Opt.* **36**, 4367–4381.
Baron, A. Q. R., Tanaka, T., Soutome, K., Takao, M., Nakamura, T., Kobayashi, K., Fujita, T., Takahashi, S., Aoyagi, H., Shimosaki, Y., Seike, T., Uchiyama, H., Ishikawa, D., Chuang, T.-H., Kimura, H., Tanaka, H., Kitamura, H. & Ishikawa, T. (2016). *AIP Conf. Proc.* **1741**, 020033.
Bazarov, I. (2012). *Phys. Rev. ST Accel. Beams*, **15**, 050703.
Chavanne, J., Van Vaerenbergh, P. & Elleaume, P. (1996). *J. Synchrotron Rad.* **3**, 93–96.
Chiu, M. S., Yang, C. H., Chao, H. C., Chang, H. P., Tsai, H. J. & Kuo, C. C. (2010). *Proceedings of the First International Particle Accelerator Conference (IPAC2010)*, Kyoto, Japan, 23–28 May 2010, pp. 4581–4583. THPE030.
Chung, T. Y., Yang, C. S., Chu, Y. L., Lin, F. Y., Jan, J. C. & Hwang, C. S. (2017). *Nucl. Instrum. Methods Phys. Res. A*, **850**, 72–77.
Coisson, R. & Walker, R. P. (1985). *International Conference on Insertion Devices for Synchrotron Sources*, Stanford, CA, USA. (Proceedings published in 1986, SPIE, Vol. 0582, pp. 24–29.)
Eriksson, M., Al-Dmour, E., Andersson, Å., Johansson, M., Leemann, S. C., Malmgren, L., Tavares, P. F. & Thorin, S. (2016). *Proceedings of the 7th International Particle Accelerator Conference (IPAC2016)*, 8–13 May 2016, Busan, Korea, pp. 11–15. MOYAA01.
Geloni, G., Kocharyan, V. & Saldin, E. (2015). *J. Synchrotron Rad.* **22**, 288–316.
Geloni, G., Saldin, E., Schneidmiller, E. & Yurkov, M. (2008). *Nucl. Instrum. Methods Phys. Res. A*, **588**, 463–493.
Goodman, J. (2015). *Statistical Optics*, p. 201. New York: John Wiley and Sons.

Hara, T., Yabashi, M., Tanaka, T., Bizen, T., Goto, S., Maréchal, X., Seike, T., Tamasaku, K., Ishikawa, T. & Kitamura, H. (2002). *Rev. Sci. Instrum.* **73**, 1125–1128.
Huang, D.-J., Chung, S.-C., Jean, Y.-C., Fung, H.-S., Lin, H.-J., Huang, Y.-S., Lee, H.-Y., Tang, M.-T., Hsu, C.-H., Lee, K., Pan, K.-Y. & Su, H.-R. (2015). Technical Design Report of the Phase-I TPS Beamlines, National Synchrotron Radiation Research Center, Hsinchu City, Taiwan.
Kim, K.-J. (1986). *Nucl. Instrum. Methods Phys. Res. A*, **246**, 71–76.
Kim, K.-J. (1989). *AIP Conf. Proc.* **184**, 565–632.
Kuo, C. C., Chen, J. Y., Chiu, M. S., Chou, P. J., Liu, Y. C., Tsai, H. J., Tseng, F. H., Hsu, K. T., Luo, G. H. & Chen, C. T. (2015). *Proceedings of the Sixth International Particle Accelerator Conference (IPAC2015)*, 3–8 May 2015, Richmond, VA, USA, pp. 1314–1318. TUXC3.
Lindberg, R. & Kim, K.-J. (2015). *Phys. Rev. ST Accel. Beams*, **18**, 090702.
Luis, A. (2007). *JEOS RP*, **2**, 07030.
Mandel, L. & Wolf, E. (1995). *Optical Coherence and Quantum Optics*, p. 188. Cambridge University Press.
Onuki, H. & Elleaume, P. (2003). *Undulators, Wigglers and their Applications*, pp. 192–193. London, New York: Taylor & Francis.
Reichardt, G., Bahrdt, J., Schmidt, J.-S., Gudat, W., Ehresmann, A., Müller-Albrecht, R., Molter, H., Schmoranzer, H., Martins, M., Schwentner, N. & Sasaki, S. (2001). *Nucl. Instrum. Methods Phys. Res. A*, **467–468**, 462–465.
Tanaka, T. (2014). *Phys. Rev. ST Accel. Beams*, **17**, 060702.
Tanaka, T. & Kitamura, H. (2001). *J. Synchrotron Rad.* **8**, 1221–1228.
Thompson, A., Vaughan, D., Kirz, J., Attwood, D., Gullikson, E., Howells, M., Kim, K.-J., Scofield, J., Liu, Y., Kortright, J., Lindau, I., Pianetta, P., Robinson, A., Underwood, J., Williams, G. & Winick, H. (2009). *X-ray Data Booklet*, http://xdb.lbl.gov/.
Walther, A. (1968). *J. Opt. Soc. Am.* **58**, 1256–1259.
Wiedemann, H. (2007). *Particle Accelerator Physics.* New York, Berlin, Heidelberg: Springer.
Wigner, E. (1932). *Phys. Rev.* **40**, 749–759.
Willeke, F. (2015). *Proceedings of the Sixth International Particle Accelerator Conference (IPAC2015)*, 3–8 May 2015, Richmond, VA, USA, pp. 11–16. MOYGB3.
Yamamoto, S., Senba, Y., Tanaka, T., Ohashi, H., Hirono, T., Kimura, H., Fujisawa, M., Miyawaki, J., Harasawa, A., Seike, T., Takahashi, S., Nariyama, N., Matsushita, T., Takeuchi, M., Ohata, T., Furukawa, Y., Takeshita, K., Goto, S., Harada, Y., Shin, S., Kitamura, H., Kakizaki, A., Oshima, M. & Matsuda, I. (2014). *J. Synchrotron Rad.* **21**, 352–365.